Spectroscopic determination of crystal-field levels in $CeRh_2Si_2$ and $CeRu_2Si_2$ and of the $4f^0$ contributions in CeM_2Si_2 (M=Cu, Ru, Rh, Pd, and Au)

T. Willers,[1] D. T. Adroja,[2] B. D. Rainford,[3] Z. Hu,[4] N. Hollmann,[4] P. O. Körner,[1,*] Y.-Y. Chin,[4] D. Schmitz,[5] H. H. Hsieh,[6] H.-J. Lin,[7] C. T. Chen,[7] E. D. Bauer,[8] J. L. Sarrao,[8] K. J. McClellan,[8] D. Byler,[8] C. Geibel,[4] F. Steglich,[4] H. Aoki,[9] P. Lejay,[10] A. Tanaka,[11] L. H. Tjeng,[4] and A. Severing[1]

[1]*Institute of Physics 2, University of Cologne, Zülpicher Straße 77, DE-50937 Cologne, Germany*
[2]*ISIS Facility, Rutherford Appleton Laboratory, Chilton, Didcot, Oxon OX11 0QX, England, United Kingdom*
[3]*Department of Physics and Astronomy, Southampton University, Southampton SO17 1BJ, England, United Kingdom*
[4]*Max Planck Institute for Chemical Physics of Solids, Nöthnizer Straße 40, DE-01187 Dresden, Germany*
[5]*Helmholtz-Zentrum Berlin für Materialien und Energie, BESSY 2, Albert-Einstein-Straße 15, DE-12489 Berlin, Germany*
[6]*Chung Cheng Institute of Technology, National Defense University, Taoyuan 335, Taiwan*
[7]*National Synchrotron Radiation Research Center, 101 Hsin-Ann Road, Hsinchu 30076, Taiwan*
[8]*Los Alamos National Laboratory, Los Alamos, New Mexico 87545, USA*
[9]*Graduate School of Science/Center for Low Temperature Science, Tohoku University, Aramaki-aza-Aoba, Aoba-ku, Sendai, Miyagi 980-8578, Japan*
[10]*Institut Néel, Centre National de la Recherche Scientifique, BP 166, FR-38042 Grenoble Cedex 9, France*
[11]*Department of Quantum Matter, ADSM Hiroshima University, Higashi-Hiroshima 739-8530, Japan*

(Received 26 August 2011; revised manuscript received 1 January 2012; published 18 January 2012)

We have determined the ground-state wave functions and crystal-field-level schemes of $CeRh_2Si_2$ and $CeRu_2Si_2$ using linear polarized soft x-ray-absorption spectroscopy (XAS) and inelastic neutron scattering. We find large crystal-field splittings and ground-state wave functions which are made of mainly $J_z = |\pm 5/2\rangle$ with some amount of $|\mp 3/2\rangle$ in both the compounds. The $4f^0$ contribution to the ground state of several members of the CeM_2Si_2 family with M = (Cu, Ru, Rh, Pd, and Au) has been determined with XAS, and the comparison reveals a trend concerning the delocalization of the f electrons. Absolute numbers are extracted from scaling to results from hard x-ray photoelectron spectroscopy on $CeRu_2Si_2$ by Yano *et al.* [Phys. Rev. B **77**, 035118 (2008)].

DOI: 10.1103/PhysRevB.85.035117 PACS number(s): 71.27.+a, 75.10.Dg, 78.70.Dm, 78.70.Nx

I. INTRODUCTION

In Kondo lattice materials two effects compete: Ruderman-Kittel-Kasuya-Yosida (RKKY) interaction, which leads to magnetic order and Kondo screening due to hybridization of $4f$ electrons with conduction electrons, which results in a non magnetic Kondo singlet ground state. Doniach has pointed out that both depend on the magnetic exchange $|J_{ex}|$ and electronic density of states at the Fermi energy $N(0)$ and that RKKY increases quadratically with the magnetic exchange so that $T_{RKKY} \propto |J_{ex}^2|N(0)$, whereas Kondo screening sets in below T_K with $T_K \propto e^{-1/|J_{ex}|N(0)}$.[1] Hence for small values of $|J_{ex}|N(0)$ magnetic order is established, while with increasing values of $|J_{ex}|N(0)$ the Néel temperature at first increases and then drops to zero, where finally the region of nonmagnetic singlet ground states is reached. The transition at 0 K is often referred to as the quantum critical point and can be realized in a given system by modifying parameters like pressure, doping, or magnetic field (see, e.g., Ref. 2)

The tetragonal cerium 122 compounds CeM_2Si_2, with M being a transition metal, cover the entire range of Doniach's phase diagram from weakly to strongly hybridized $4f$ electrons,[3] with some of the compounds close to the quantum critical point.[4–6] $CeRu_2Si_2$ is the most itinerant compound of the series without exhibiting magnetic order or superconductivity down to 3 mK.[7,8] Metamagnetism develops when a field of $H_M = 7.7$ T is applied.[7] This metamagnetism in $CeRu_2Si_2$ has been intensively studied for a long time.[6,9–11] A small expansion of the volume by alloying with La, Ge, or Rh induces magnetic order, showing the proximity to a quantum critical point.[12–14] The large linear coefficient of the temperature-dependent specific heat $\gamma \approx 350$ mJ/mol K^2, a T_K of the order of 15 to 25 K,[12,15–19] and also techniques like de Haas-van Alphen[20] point toward the itinerant nature of the f electrons in $CeRu_2Si_2$.

The corresponding presence of $4f^0$ is supported by L_{III} x-ray absorption[21] and hard x-ray photoelectron spectroscopy (HAXPES).[22] In contrast, $CeRh_2Si_2$ has an exceptionally high ordering temperature of $T_N = 37$ K, followed by a second magnetic transition at 26 K,[23–26] which points toward the presence of strong RKKY interactions. Yet, despite the high ordering temperature, magnetic order breaks down when applying only 10 kbars of pressure and superconductivity develops below 400 mK.[27–29] For comparison, $CePd_2Si_2$ orders antiferromagnetically at $T_N = 10$ K and requires a three-times-higher pressure to suppress magnetic order and establish superconductivity.[30,31] The fact that T_N in both compounds is pressure sensitive places them in the intermediate coupling (J_{ex}) regime, where the Kondo effect competes with magnetic ordering, but more so in $CeRh_2Si_2$ than $CePd_2Si_2$. In the presence of magnetic order it is not obvious to give a value for the Kondo temperature T_K. For example the quasielastic linewidth $\Gamma/2$ in inelastic neutron scattering can only be measured in the paramagnetic phase. At 40 K in the paramagnetic phase the quasielastic linewidths (HWHM) of $CeRh_2Si_2$ and itinerant $CeRu_2Si_2$ have about the same linewidth ($\Gamma/2 \approx 30$ K at $T = 40$ K), while the linewidth of $CePd_2Si_2$ is half of this value ($\Gamma/2 \approx 15$ K at

$T = 40$ K).[17] A recent specific-heat and electrical study of the dilution series $Ce(Rh_{1-x}Pd_x)Si_2$ supports the current picture of an itinerant type of magnetic order in $CeRh_2Si_2$ in contrast to the localized antiferromagnetic state as in $CePd_2Si_2$.[32] Also, the resistivity of $CeRh_2Si_2$ exhibits an important contribution of Kondo scattering[33] and L_{III} edge data show the presence of some $4f^0$.[21] De Haas-van Alphen experiments on $CeRh_2Si_2$ infer that the $4f$ electrons are localized at ambient pressure. Above p_c, however, they do contribute to the Fermi surface and can be described within an itinerant band model.[34]

Hence it seems that $CeRh_2Si2$ and $CeRu_2Si_2$ are on either side of the quantum critical point in Doniach's phase diagram, the former in the regime of dominating RKKY and the latter in the range of strong coupling where the Kondo prevails.

From dc magnetic susceptibility and isothermal magnetization measurements it was suggested[35,36] that the ground state of $CeRu_2Si_2$ is close to the Ising-type pure $J_z = |\pm 5/2\rangle$, later supported by magnetic form-factor measurements.[37] We recall that the Hund's rule ground state of Ce^{3+} with $J = 5/2$ splits under the influence of a tetragonal crystal field (point group D_{4h}) into three Kramer's doublets, which can be represented in the basis of $|J_z\rangle$. The eigenfunctions of the three Kramer's doublets can be written as

$$\begin{aligned} |2\rangle &= \Gamma_6 = \quad |\pm 1/2\rangle, \\ |1\rangle &= \Gamma_7^2 = \beta|\pm 5/2\rangle \pm \alpha|\mp 3/2\rangle, \\ |0\rangle &= \Gamma_7^1 = \alpha|\pm 5/2\rangle \mp \beta|\mp 3/2\rangle, \end{aligned} \tag{1}$$

with $\alpha^2 + \beta^2 = 1$. Within the Hund's rule ground state the mixing parameter α and the transition energies ΔE_1 and ΔE_2 between ground and excited crystal-field states fully determine the crystal-field Stevens parameters B_2^0, B_4^0, and B_4^4 in the crystal-field Hamiltonian $H_{CF} = B_2^0 O_2^0 + B_4^0 O_4^0 + |B_4^4| O_4^4$.[38] Macroscopic and high-resolution photoemission experiments suggest level splittings of the order of 18 to 33 meV in $CeRu_2Si_2$.[19,35] According to dc magnetic susceptibility data the ground state of $CeRh_2Si_2$ should also have a large $J_z = |\pm 5/2\rangle$ contribution ($\alpha = 0.9 - 0.98$) and a large level splitting of about 25 to 60 meV.[33,39] The large energy splittings in the Ru and Rh compound are supported by theoretical work where the splittings were calculated by means of an *ab initio* many-body combined technique.[40] However, although the low-energy excitations of $CeRu_2Si_2$ were investigated in great detail,[16,17] there are no thermal inelastic neutron-scattering data available for either of the two compounds to confirm the ground-state wave functions or level splittings.

Since the near-ground-state properties of heavy fermions evolve out of the $4f$ electrons which are hybridized with the conduction electrons, knowledge of the $4f$ wave function and the low-energy splittings is essential for modeling these compounds. Here we determine spectroscopically the crystal-field ground-state wave functions of $CeRu_2Si_2$ and $CeRh_2Si_2$ and also the energies of the crystal-field splittings. Further, the degree of delocalization is investigated in order to sort the members of the CeM_2Si_2 according to their itineracy.

We use the linear dichroism (LD) in soft x-ray-absorption spectroscopy (XAS) to determine the crystal-field ground states of $CeRu_2Si_2$ and $CeRh_2Si_2$. The dipole selection rules in the absorption process with linear polarized light give sensitivity to the initial-state symmetry, and it has been applied successfully at the cerium $M_{4,5}$ edges to determine the ground-state wave functions of crystal-field-split tetragonal cerium compounds.[41–43] At sufficiently low temperatures only the ground state is probed. We also present temperature-dependent XAS measurements because the change of polarization due to thermal population of higher lying crystal-field states gives an estimate of the crystal-field splittings.[41–43] Finally, the crystal-field transition energies are determined with thermal inelastic neutron scattering.

A powerful tool to determine the $4f^0$ contribution is HAXPES, but so far for the CeM_2Si_2 family only HAXPES data of $CeRu_2Si_2$ are available.[22] However, the fingerprint of the $4f^0$ contribution in the ground state can also be seen in the XAS spectra. The spectral weight of the absorption process, $3d^{10}4f^0 \rightarrow 3d^9 4f^1$, next to the main absorption due to $3d^{10}4f^1 \rightarrow 3d^9 4f^2$, is representative for the $4f^0$ contribution to the initial state,[44,45] and in Ref. 22 the $4f^0$ spectral weight obtained from HAXPES has been consistently fitted to nonpolarized XAS data of $CeRu_2Si_2$. In the present study we compare the $4f^0$ spectral weights in the isotropic XAS spectra of several members of the CeM_2Si_2 (M = Cu, Ru, Rh, Pd, and Au) series, and absolute values are obtained by scaling the XAS $4f^0$ amount to the $CeRu_2Si_2$ HAXPES result by Yano *et al.*[22]

II. EXPERIMENTAL

High-quality single crystals of $CeCu_2Si_2$, $CeRu_2Si_2$, $CeRh_2Si_2$, $CePd_2Si_2$, and $CeAu_2Si_2$ for the x-ray experiments were grown with the Czochralski technique and oriented with Laue diffraction. The polycrystalline samples for the neutron-scattering experiments were prepared using the standard arc melting technique on a water cooled copper hearth under the titanium gettered inert argon atmosphere using the high-purity elements (Ce,La: 99.9% Ru/Rh: 99.99% Si: 99.999%) in a stoichiometric ratio. During the melting process the samples were flipped and remelted several times to achieve homogeneity. Further, to improve homogeneity and reduce possible disorder, the as-cast samples were wrapped in tantalum foil and annealed for a week at 900°C under a dynamic vacuum. The crystal structure and phase purity were checked by powder x-ray diffraction and neutron diffraction.

The XAS data were taken at the synchrotron light sources Helmholtz Zentrum Berlin BESSY II in Germany and the National Synchrotron Radiation Research Center (NSRRC) in Taiwan. The spectra were recorded with the total electron yield (TEY) method in a ultra-high-vacuum chamber with a pressure of several 10^{-10} mbars. The TEY signal was normalized to the incoming flux I_0 as measured at the refocusing mirror (BESSY) or on a Au mesh (NSRRC) in front of the sample. Clean sample surfaces were obtained by cleaving the single crystals *in situ*. At BESSY II the UE46 PGM-1 undulator beam line was used and the energy resolution at the $M_{4,5}$ edges ($h\nu \approx 875 - 910$ eV) was set to 0.15 eV. The undulator beam line allows for a change of polarization without changing the probing spot on the sample surface. The two polarizations were $E \perp c$ and $E \parallel c$, c being the long tetragonal axis. At NSRRC the experiment was performed at the Dragon bending magnet beam line. Here the energy resolution for the same energy range was set to 0.4 eV. The crystals were mounted with the c

axis perpendicular to the Poynting vector so that rotating the crystal around this Poynting vector realized an electric-field variation from $E \perp c$ to $E \parallel c$. For all measurements the sample was rotated four times by 90° so that for each orientation $E \perp c$ and $E \parallel c$ two equivalent positions were measured. Several crystals were measured and/or recleaved so that the reproducibility of the data is assured.

The spectra were simulated with the full multiplet calculations based on the XTLS 8.3 program[46] as described elsewhere.[41–43] All atomic parameters are given by Hartree-Fock values with typical reduction factors of about 40% for the $4f$-$4f$ Coulomb interactions and about 20% for the $3d$-$4f$ interactions. These values reproduce best the isotropic spectra, $I_{\text{isotropic}} = 2I_{E\perp c} + I_{E\parallel c}$.

During separate beam times the neutron-scattering functions $S(Q,\omega)$ of the $CeRh_2Si_2$ and $CeRu_2Si_2$ powder samples were measured with the inelastic time-of-flight high-energy transfer spectrometer (HET) at the neutron spallation source, ISIS Facility, UK. $CeRu_2Si_2$ was measured with incoming energies of E_o = 20 and 70 meV and $CeRh_2Si_2$ with E_o = 20 and 100 meV. The energy resolutions are 0.6, 1.8, and 2.0 meV at elastic scattering in the 2.5-m detector bank for either incoming energy. The low-angle detector grouping covers 2θ = 9–20° for the 20-meV and 11–18° for the 100 meV Rh data and 2θ = 9–24° and 8–24° for the 20- and 70-meV Ru data. All high-angle data are grouped from 2θ = 125–138°. We therefore refer to $S(2\theta,\omega)$ from now on. $LaRu_2Si_2$ has been measured as an isostructural, nonmagnetic reference compound. The powder samples were mounted in a closed cycle refrigerator (CCR) which reached a base temperature of 5 K. The powder samples of $CeRu_2Si_2$ and $LaRu_2Si_2$ amounted to about 35 g each, while to limit an absorption problem only 13 g of the $CeRh_2Si_2$ sample was used. All data have been normalized to monitor count rate and vanadium and have been corrected for absorption and self-shielding. The phonon scattering has been identified using a high- to low-angle scaling factor which was determined empirically from the La measurements, following the method described by Murani.[47]

III. RESULTS

A. Ground-state wave functions with low-temperature polarized soft XAS

The thick lines at the bottom of either panel in Fig. 1 show the polarized soft XAS data of $CeRh_2Si_2$ and $CeRu_2Si_2$ at low temperatures. The red lines were measured for light polarized parallel and the blue lines for light perpendicular to the tetragonal c axis. The M_5 edge at 883 eV as well as the M_4 edge at 900 eV show a strong polarization effect which is not consistent with a pure J_z state for either sample (see the simulations of pure J_z states in Refs. 41 and 42). Though similar, some differences show when comparing the Ru and Rh data in detail: At the M_5 edge the intensity ratios of the high- and low-energy peaks in the E$\|c$ data (red lines) are different, as are the intensity ratios of the higher-energy peak of the E$\|c$ (red lines) and the low-energy shoulder in the the E$\perp$c (blue lines) data. The comparison with XAS simulations for $\alpha^2 = 0$ to 1 (see Fig. 2 in Ref. 41) shows that the data

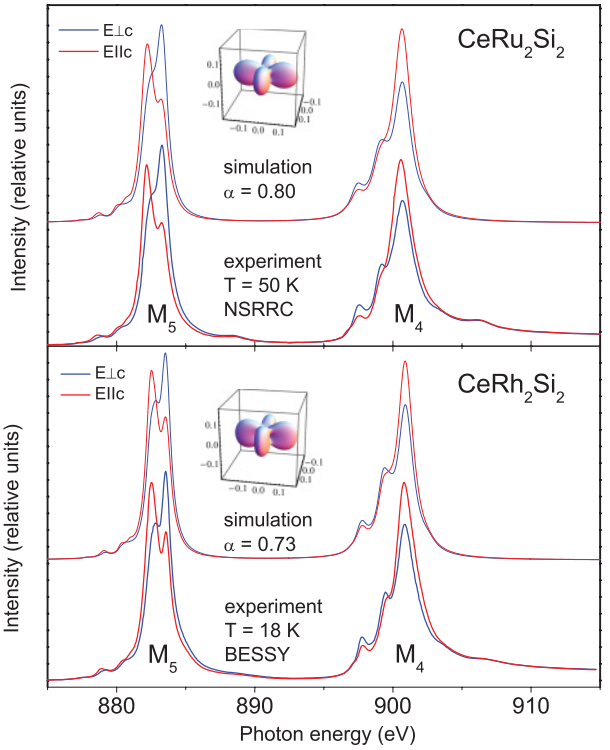

FIG. 1. (Color online) Low-temperature linear polarized XAS spectra of $CeRu_2Si_2$ and $CeRh_2Si_2$ at the $M_{4,5}$ absorption edge. The thick lines are experimental data, and the thin lines are simulations as described in the text. The orbitals represent the spatial distribution of the $4f$ wave function for either ground state.

are consistent with mixed $|\mp 3/2\rangle$ and $|\pm 5/2\rangle$ states, with a slightly larger J_z=$|\pm 5/2\rangle$ contribution in the Ru sample. We have now simulated the XAS data with the above-mentioned full multiplet routine, and good data descriptions are obtained for the wave functions given in Eq. (2) within delta $\Delta\alpha = \pm 0.02$ (see the thin lines in Fig. 1). The respective angular distributions of the $4f$ electrons are shown as insets:

$$\begin{aligned} &CeRu_2Si_2: \quad |0\rangle = \Gamma_7^1 = 0.80|\pm 5/2\rangle \mp 0.60|\mp 3/2\rangle, \\ &CeRh_2Si_2: \quad |0\rangle = \Gamma_7^1 = 0.73|\pm 5/2\rangle \mp 0.68|\mp 3/2\rangle. \end{aligned} \tag{2}$$

The absorption edges were also measured at elevated temperatures (see the legend in the left column of Fig. 2) in order to verify that the 18- and 20-K data reflect the ground state. When excited states get populated the measured polarization is given by a weighted superposition of the polarization from either state. At 100 K an excited state at 10 meV would have a population of about 25%; i.e., it should contribute to the polarization, but there is clearly no change in polarization between 20 and 100 K. We therefore conclude that the polarization in the XAS data at 18 and 20 K reflects the ground-state wave function and that there are no excited crystal-field levels below 10 meV.

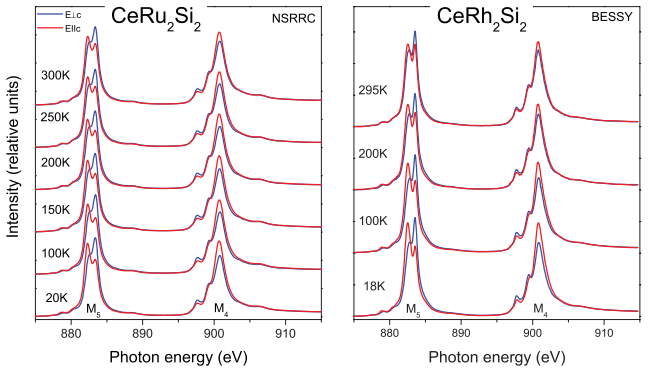

FIG. 2. (Color online) Temperature dependence of the M_4 and M_5 absorption edges of $CeRh_2Si_2$ and of $CeRu_2Si_2$ for light polarized parallel and perpendicular to the long c axis.

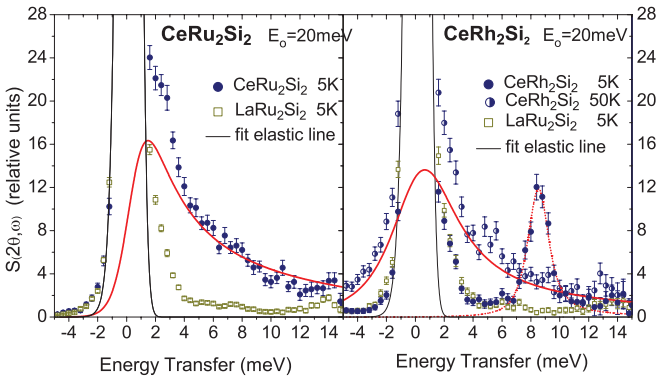

FIG. 3. (Color online) Inelastic neutron data of $CeRh_2Si_2$ and of $CeRu_2Si_2$ with 20-meV incident energy; full blue dots are 5-K data and half-filled blue dots are 50-K data. The open green squares are scattering from $LaRu_2Si_2$. The solid red lines in the $CeRu_2Si_2$ at 5 K and $CeRh_2Si_2$ data at 50 K are quasielastic Lorentzians to describe the magnetic scattering, and the dashed red line is an inelastic line for the magnon scattering in $CeRh_2Si_2$ at 5 K. The scattering near 2 meV in the La and Ce data is due to secondary scattering from the CCR walls.

B. Crystal-field transition energies with INS and temperature-dependent polarized soft XAS

Figure 3 shows the low-angle neutron data with 20-meV incident energy for $CeRu_2Si_2$ at 5 K and for $CeRh_2Si_2$ at 5 and 50 K (blue dots). The respective $LaRu_2Si_2$ measurements are also shown (open green squares). The black lines indicate the elastic scattering. There is some extra scattering in the La data at about 2 meV which is not accounted for by the elastic line, most likely due to secondary scattering from the CCR walls. It is sample dependent and appears in all the 20-meV data. Nevertheless there is clearly additional scattering in the cerium data which is not present in the La spectra and can therefore be attributed to magnetic scattering. The magnetic scattering in the ruthenium data is well described with a 1.2-meV-wide (HWHM) quasielastic Lorentzian, in accordance with previous publications.[16,17,48] The magnetic scattering of paramagnetic $CeRh_2Si_2$ at 50 K looks very similar and can be described with a quasielastic Lorentzian with $\Gamma/2 \approx 3$ meV, also in agreement with previous work.[17] At 5 K, however, $CeRh_2Si_2$ exhibits inelastic scattering around 8.5 meV instead of quasielastic scattering. It is assigned to magnon scattering because at 5 K $CeRh_2Si_2$ is magnetically ordered, and we expect spin waves below T_N. These 20-meV data show, in agreement with the lack of any temperature dependence in the XAS data up to 100 K, that there are no low-lying crystal-field transitions (below 15 meV). The full blue dots in Fig. 4 show the scattering functions of $CeRu_2Si_2$ and $CeRh_2Si_2$ with 70- and 100-meV incident energy for low angles and low temperatures. Note that the resolution is different due to the different incident energies. The total scattering is broadly distributed up to 60 meV, and it is not evident at first sight how to separate magnetic and phonon scattering. $CeRh_2Si_2$ was also measured in the paramagnetic phase at 50 K, but no change in the inelastic broad scattering intensity above 20 meV was observed. We therefore analyze the low-temperature data based on the crystal-field model, without taking into account the spin-wave contribution.

The two top panels of Fig. 5 show the phonon scattering in the high-angle detectors of the two cerium samples (blue dots) and of the respective $LaRu_2Si_2$ runs (open green squares). The high- to low-angle scattering works out rather well, although the phonon scattering of all three samples is not identical, in intensity because of the different scattering lengths of Ce and La, Rh and Ru, and in energy because of the different lattice constants and atomic distances in the Ru and Rh compound. For 70- and 100-meV incident energy the high-angle La data are scaled to low angles with empirically determined scaling factors of 0.245 for $E_o = 70$ meV and of 0.166 for $E_o = 100$ meV. Above 10-meV energy transfer the scaled high-angle scattering (open green squares) compares well with the low-angle scattering (full green squares). However, it should be noted that especially for 70-meV incident energy this scaling underestimates the phonon scattering in the low-angle spectra below 10 meV.

Applying this type of scaling to the cerium data gives the open blue dots in Fig. 4, and they represent the phonon contribution to the total scattering in the low-angle detectors. The difference of total and scaled phonon intensity should be purely magnetic. The Rh data show some inelastic scattering just below 10 meV, and it can be attributed to magnon scattering as mentioned previously. In contrast, the supplement intensity below 10 meV in the Ru data cannot be accounted for by the quasielastic scattering, but, as has been shown by means of the La data, the phonon correction from scaling underestimates the phonon scattering at energy transfers smaller than 10 meV. But as shown above the temperature dependent XAS and 20-meV neutron data already rule out any crystal-field excitations in this energy window. At 30 and possibly just above 50 meV is also some extra scattering, and this is due to crystal-field excitations. The inelastic magnetic scattering is now fitted to a crystal-field model by taking into account the ground-state wave function as determined with XAS. The wave functions determine the ratio of the crystal-field transition intensities and therefore minimize the number of free fit parameters. The crystal-field excitations (see the red lines in Fig. 4) were obtained by keeping the intensity ratios and phonon scaling factor fixed and restricting the fitting region to energy transfers larger than 10 meV. $CeRu_2Si_2$ is best described with a quasiquartet at 32 meV, similar to $CeCu_2Si_2$,[49] and $CeRh_2Si_2$ is best fitted with the strong Γ_7^1-to-Γ_7^2 transition

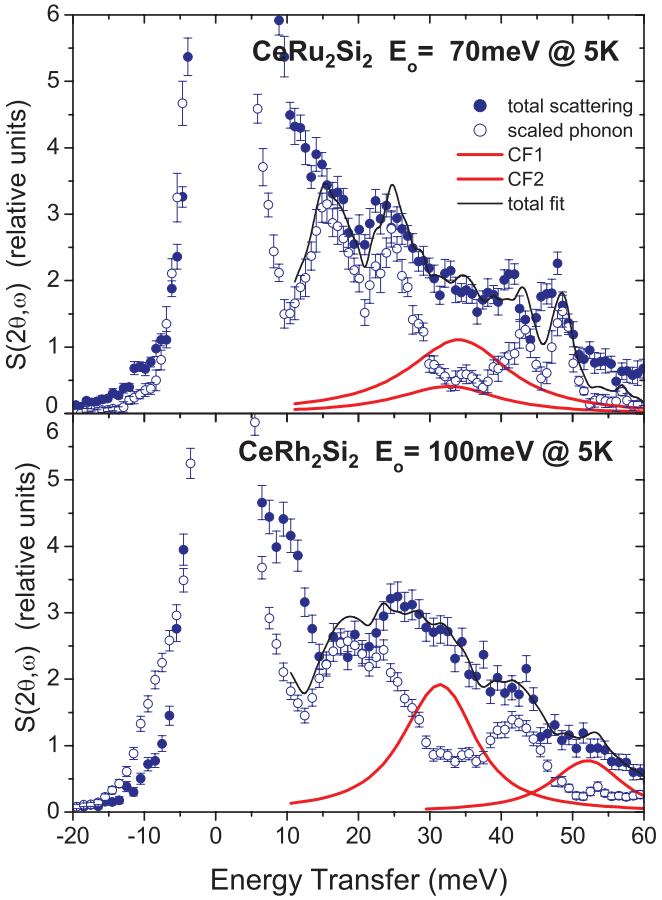

FIG. 4. (Color online) Inelastic neutron data at 5 K of $CeRh_2Si_2$ with 100-meV and of $CeRu_2Si_2$ with 70-meV incident energy (full blue dots). The open blue dots reflect the phonon scattering and originate from scaling the high to low angles. The magnetic intensity is the difference of total and scaled phonon scattering (see text). The red lines are the results of a crystal-field fit. The black lines are the sum of the scaled phonon data and crystal-field intensity. Note that the scattering below 10 meV in $CeRh_2Si_2$ is due to spin waves.

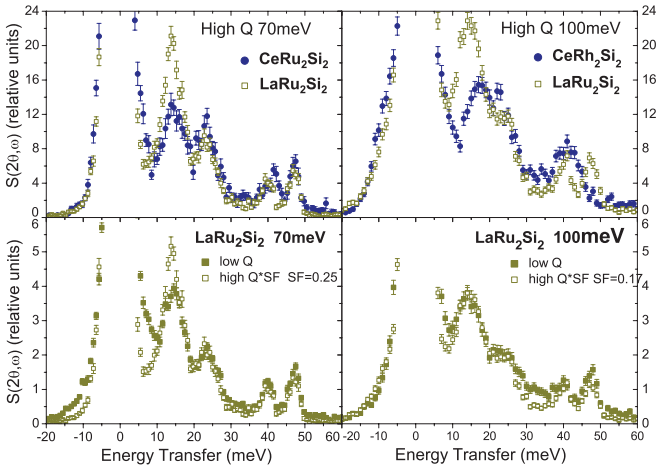

FIG. 5. (Color online) Top: Comparison of high-angle cerium and lanthanum data. Bottom: Comparison of scaled high-angle and low-angle lanthanum data for 70- and 100-meV incident energy.

TABLE I. Linewidths of the crystal-field excitations and transition energies from fitting a crystal-field model to the magnetic scattering in the 70- and 100-meV neutron data. $I_{<|>}$ refers to the calculated transition intensities when adopting the ground-state wave function as determined from XAS. B_n^m are the Steven's crystal-field parameters.

$T = 5$ K	$CeRh_2Si_2$	$CeRu_2Si_2$
Γ_{in}	5.1 meV	8.5 meV
ΔE_1	30 meV	33 meV
$I_{\langle\Gamma_7^2\|\Gamma_7^1\rangle}$	1.78 b	1.53 b
ΔE_2	52 meV	32 meV
$I_{\langle\Gamma_6\|\Gamma_7^1\rangle}$	0.83 b	0.64 b
B_2^0	−1.83 meV	−1.07 meV
B_4^0	0.08 meV	0.015 meV
B_4^4	±0.56 meV	±0.59 meV

at 30 meV and the weaker Γ_7^1-to-Γ_6 transition at 52 meV. The corresponding fit parameters are listed in Table I. In both compounds the crystal-field excitations are broader than the resolution due to the Kondo effect.[49] The $CeRu_2Si_2$ data could also be described with the weak transition above 50 meV and only one doublet at about 30 meV; however, here we present the best possible fit.

The temperature dependence of the polarized XAS data in Fig. 2 supports the above crystal-field level schemes. The non-negligible LD at room temperature shows that the excited crystal-field states are only partially populated, i.e., that the level splitting must be large. The room temperature LD is actually in agreement with the superimposed polarizations of the ground state and partially populated Γ_7^2 and Γ_6 states. Here the crystal-field energy splittings enter into the calculation via the thermal occupation.

C. $4f^0$ contribution from isotropic XAS

Figure 6 shows isotropic XAS data of several members of the CeM_2Si_2 family with M = Cu, Ru, Rh, Pd, and Au. The arrows at 888 and 906 eV point out the spectral weights due to the $4f^0$ contribution in the ground state. The humps are most pronounced for $CeRu_2Si_2$ and practically nonexistent for $CeAu_2Si_2$, and their spectral weight decreases with temperature. In order to compare the $4f^0$ spectral weights more quantitatively, the isotropic XAS have been normalized such that the main edges match and then a linear background has been subtracted (see the black lines in Fig. 6). The results of this background subtraction are shown in Fig. 7 for the M_4 and M_5 edges, and the spectral weights are determined by integration from 887 to 890 eV and 905 to 908 eV, respectively (see Table II). $CeRu_2Si_2$ has clearly the strongest $4f^0$ component, followed by $CeCu_2Si_2$, $CeRh_2Si_2$, and finally $CePd_2Si_2$. In $CeAu_2Si_2$ the $4f^0$ contribution is so small that it cannot be identified. Absolute numbers are obtained by scaling the $4f^0$ contribution in the $CeRu_2Si_2$ XAS data at 20 K to 6%. This value was determined with HAXPES at the same temperature by Yano *et al.*[22] We note that for each compound the M_5 and M_4 integrals consistently produce the same $4f^0$ number.

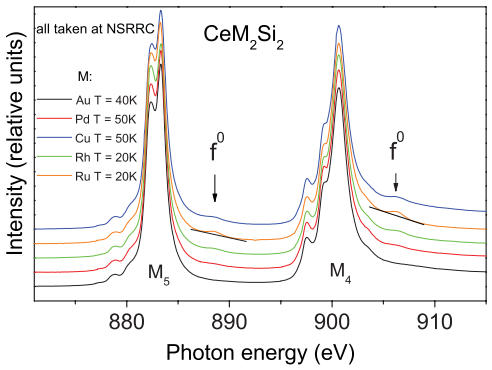

FIG. 6. (Color online) Isotropic XAS data at the M_4 and M_5 edges of several compounds of the CeM_2Si$_2$ series. The arrows point out the $4f^0$ spectral weights.

IV. DISCUSSION

The ground-state wave functions of $CeRu_2Si_2$ and $CeRh_2Si_2$ have been determined with XAS, and the resulting wave functions were found to have a larger $J_z=|\pm 5/2\rangle$ than $J_z=|\mp 3/2\rangle$ contribution in contrast to $CePd_2Si_2$[41,50] but considerably less $|\pm 5/2\rangle$ than predicted from the anisotropies of the high-temperature static susceptibility.[33,35,39] The smaller than expected $J_z = |\pm 5/2\rangle$ contributions give rise to smaller anisotropies in the static susceptibility, but when analyzing static susceptibility measurements it should be considered that molecular and/or exchange fields, which are possibly anisotropic, influence the high-temperature anisotropy and may disguise the true wave function. An anisotropic Kondo interaction will have the same effect. In contrast, the LD in XAS does not change when going through the magnetic ordering transition in $CeRh_2Si_2$ (see Fig. 2), which implies that the LD reflects the wave function, being independent of magnetic interactions. Also, in $CeRu_2Si_2$ the LD for temperatures close to the Kondo temperature is the same as, e.g., at 100 or 150 K (see Fig. 2), which suggests that also the Kondo effect does not influence the crystal-field result.

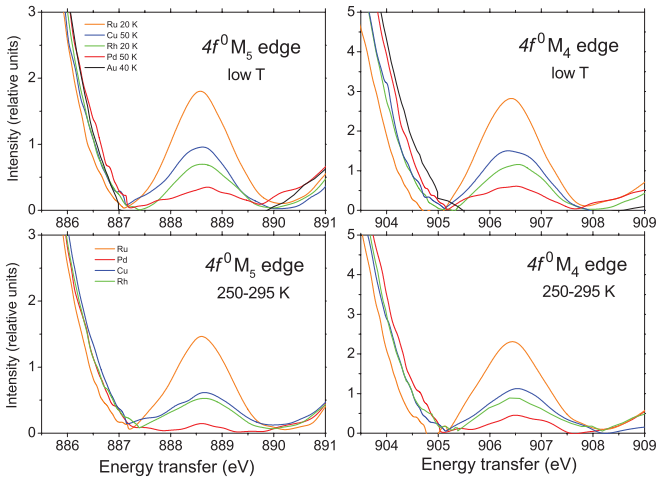

FIG. 7. (Color online) $4f^0$ intensities at the M_4 and M_5 edges after subtraction of a linear background for low and high temperatures. The exact low temperature is specified in the top left figure.

TABLE II. Integrated intensities of $4f^0$ humps at the M_4 and M_5 edges in relative intensity units times eV for low and high temperatures. The percent values result from scaling the low-temperature XAS f^0 contribution of $CeRu_2Si_2$ to the 6% $4f^0$ contribution which was determined for the same temperature in a HAXPES experiment by Yano *et al.*[22]

	T (K)	M_5 integral 887–890 eV	$4f^0$	M_4 integral 905–908 eV	$4f^0$
$CeRu_2Si_2$	20	2.5	6%	4.0	6%
$CeCu_2Si_2$	50	1.3	3%	2.2	3%
$CeRh_2Si_2$	20	0.94	2.3%	1.6	2.4%
$CePd_2Si_2$	50	0.5	1.2%	0.9	1.4%
$CeAu_2Si_2$	40	–	–	–	–
$CeRu_2Si_2$	295	2.0	4.8%	3.4	5.1%
$CeCu_2Si_2$	250	1.0	2.4%	1.8	2.7%
$CeRh_2Si_2$	295	0.8	1.9%	1.4	2.1%
$CePd_2Si_2$	295	(0.2)	(0.5)%	0.6	0.9%

For $CeRh_2Si_2$ the crystal-field ground-state wave function given above corresponds to magnetic moments of $\mu_{\mathrm{XAS}}^{\|c} = 0.53$ and of $\mu_{\mathrm{XAS}}^{\|ab} = 0.93\ \mu_B$. Note that these values have been calculated taking into account an infinitesimally small magnetic field. An exchange field could yield larger moments, because when sufficiently large it stabilizes the larger J_z in the bottom Zeeman level of the ground state, i.e., $J_z = |\pm 5/2\rangle$ over $|\mp 3/2\rangle$. An exchange field of 300 T would give a moment of about $\mu^{\|c} = 1.05$ and $\mu^{\|ab} = 1.00\ \mu_B$. The highest possible moment for a Γ_7 ground state amounts to $\mu^{\|c} = 2.14\ \mu_B$ for a pure $J_z = |\pm 5/2\rangle$ ground state. $CeRh_2Si_2$ orders antiferromagnetically along c, and reported values for the ordered moments are 0.3 μ_B from NMR measurements[51] and 1.7 to 2.4 μ_B from neutron diffraction.[24,26] The large differences were attributed to the different time scales of the two techniques, thereby suggesting a dynamic nature of the f electron moments.[26] It should also be noted that the magnetic structure has not been conclusively determined. For $CeRu_2Si_2$ the ground-state wave function from XAS yields $\mu_{\mathrm{XAS}}^{\|c} \approx \mu_{\mathrm{XAS}}^{\|ab} \approx 0.9\ \mu_B$.

Previous neutron data which gave a value for the quasielastic linewidths of $CeRh_2Si_2$ above the ordering transition were measured with cold neutrons in up-scattering, which can be ambiguous when the linewidths are broad with respect to the thermal energy k_BT.[17] Here we determine the quasielastic linewidth at 40 K with a neutron energy-loss experiment and find consistent results. Further measurements of $CeRu_2Si_2$ with 20-meV incident energy at elevated temperatures (not shown) confirm that at 40 K the quasielastic linewidths of both compounds are comparable, implying that also the Kondo scales (k_BT_K) are of the same order. However, it should be noted that at 5 K the inelastic linewidths in $CeRu_2Si_2$ are considerably larger than in $CeRh_2Si_2$ (see Table I).

In Table II the $4f^0$ spectral weights for each CeM_2Si$_2$ compound are given as determined from the isotropic XAS spectra. According to Bickers *et al.*[52] the temperature variation of n_f can be large, so that a comparison for different compounds should be done for similar effective T/T_K values

or for temperatures where one is either in the *low*- ($T/T_K \ll 1$) or *high*-temperature regime ($T/T_K \gg 1$). The XAS data of $CeRu_2Si_2$ and $CeRh_2Si_2$ were both taken at 20 K, and their Kondo temperatures as discussed above are comparable and of the order of 30 K. Hence the f^0 numbers given in Table II refer to the same low-temperature regime. $CePd_2Si_2$ and $CeCu_2Si_2$ were both measured at 50 K, and according to Refs. 17 and 49 the Kondo temperatures are of the order of 10 and 10–20 K. So here f^0 values are given for the high-temperature regime. The two sets of data, Ru/Rh versus Pd/Cu, referring to different T/T_K regimes, give a trend for the f^0 occupation which is confirmed by the high-temperature regime of all four compounds (see the bottom in Fig. 7 and Table II); i.e., also at high temperatures the f^0 contribution is largest for the Ru compound, followed by Cu and Rh, and finally smallest for Pd.

The $4f^0$ spectral weights in XAS show agreement with previous investigations that $CeRu_2Si_2$, which exhibits neither magnetism nor superconductivity, is the most delocalized compound within the CeM_2Si_2 series, followed by $CeCu_2Si_2$, which is at the border of itinerant magnetic order and superconductivity depending on stoichiometry.[53] $CeRh_2Si_2$ shows an important amount of $4f^0$, which is comparable to $CeCu_2Si_2$. Actually, the pressure sensitivity of the Néel temperatures of $CeRh_2Si_2$, $CePd_2Si_2$, and $CeAu_2Si_2$ follow the $4f^0$ occupancy; i.e., the more $4f^0$ the more pressure sensitive is T_N. For $CeAu_2Si_2$ the magnetic order is pressure resistant.[27,54] The comparable $4f^0$ contributions of $CeRh_2Si_2$ and $CeCu_2Si_2$, but the much higher ordering temperature of the former, confirm that $CeRh_2Si_2$ must be close to the maximum in Doniach's phase diagram, not far from the quantum critical point, and that $CeCu_2Si_2$ is even closer to the zero point where the magnetic order occurs in the Kondo screened regime with a large Fermi surface. $CePd_2Si_2$ and $CeAu_2Si_2$ are clearly in the regime of smaller $|J_{ex}|N(0)$ values, where RKKY interaction and Kondo screening are weaker. These findings are in agreement with previous studies (see, e.g., Ref. 55 and references therein), but here we show in a direct spectroscopic comparison how the CeM_2Si_2 can be sorted according to their degree of f electron delocalization.

V. SUMMARY

The ground-state wave functions of $CeRh_2Si_2$ and $CeRu_2Si_2$ which have been determined with linear polarized XAS have more $J_z = |\pm 5/2\rangle$ than $J_z = |\mp 3/2\rangle$ character. The crystal-field splittings are large in both compounds. The best fit to the $CeRu_2Si_2$ neutron data was obtained for a quasiquartet at about 32 to 33 meV and for $CeRh_2Si_2$ for the Γ_7^1-to-Γ_7^2 transition at 30 meV and the Γ_7^1-to-Γ_6 transition at 52 meV. The $4f^0$ contributions of the CeM_2Si_2 (M = Ru, Rh, Pd, Cu, and Au) have been determined from the isotropic XAS data. We find that the f electrons become increasingly delocalized from M = Au, to Pd, Rh, and Cu, and are maximum itinerant for M = Ru.

ACKNOWLEDGMENTS

We thank M. W. Haverkort for providing the CrystalFieldTheory package for Mathematica used to calculate the wave-function density plots. T.W. and N.H. were partially supported by the Bonn-Cologne Graduate School of Physics and Astronomy and part of the work was funded by DFG project AOBJ 583872.

*Present address: Institute for Physical Chemistry, University of Cologne, Luxenburger Str. 166, DE-50939 Cologne, Germany.

[1] S. Doniach, Physica B **91**, 231 (1977).
[2] P. Gegenwart, Q. Si, and F. Steglich, Nature Physics **4**, 186 (2008).
[3] T. Endstra, G. J. Nieuwenhuys, and J. A. Mydosh, Phys. Rev. B **48**, 9595 (1993).
[4] J.-H. She, J. Zaanen, A. R. Bishop, and A. V. Balatsky, Phys. Rev. B **82**, 165128 (2010).
[5] J. Flouquet, D. Aoki, W. Knafo, G. Knebel, T. Matsuda, R. Raymond, C. Proust, C. Paulsen, and P. Haen, J. Low Temp. Phys. **161**, 83 (2010).
[6] D. Aoki, C. Paulsen, T. Matsuda, L. Malone, G. Knebel, P. Haen, P. Lejay, R. Settai, Y. Ōnuki, and J. Flouquet, J. Phys. Soc. Jpn. **80**, 053702 (2011).
[7] P. Haen, J. Flouquet, F. Lapierre, P. Lejay, and G. Remenyi, J. Low Temp. Phys. **67**, 391 (1987).
[8] J. Flouquet, S. Kambe, L. P. Regnault, P. Haen, J. P. Brison, F. Lapierre, and P. Lejay, Physica B: Condensed Matter **215**, 77 (1995).
[9] J. Flouquet, P. Haen, S. Raymond, D. Aoki, and K. G., Physica B **319**, 215 (2002).
[10] J. Flouquet, Prog. Low Temp. Phys. **15**, 139 (2005).
[11] F. Weickert, M. Brando, F. Steglich, P. Gegenwart, and M. Garst, Phys. Rev. B **81**, 134438 (2010).
[12] R. Fisher, C. Marcenat, N. Phillips, P. Haen, F. Lapierre, P. Lejay, J. Flouquet, and J. Voiron, J. Low Temp. Phys. **84**, 49 (1991).
[13] P. Haen, F. Mallmann, M.-J. Besnus, J.-P. Kappler, F. Bourdarot, P. Burlet, and T. Fukuharam, J. Phys. Soc. Jpn. **65**, 16 (1996).
[14] J. S. Kim, D. J. Mixson, D. Burnette, B. Andraka, K. Ingersent, G. R. Stewart, E. W Scheidt, and W. Scherer, Phys. Rev. B **74**, 165112 (2006).
[15] A. Amato, D. Jaccard, J. Sierro, F. Lapierre, P. Haen, P. Lejay, and J. Flouquet, J. Magn. Magn. Mater. **76–77**, 263 (1988).
[16] L. P. Regnault, W. A. C. Erkelens, J. Rossat-Mignod, P. Lejay, and J. Flouquet, Phys. Rev. B **38**, 4481 (1988).
[17] A. Severing, E. Holland-Moritz, and B. Frick, Phys. Rev. B **39**, 4164 (1989).
[18] A. Sekiyama *et al.*, J. Phys. Soc. Jpn. **69**, 2771 (2000).
[19] D. Ehm, S. Hüfner, F. Reinert, J. Kroha, P. Wölfle, O. Stockert, C. Geibel, and H. v. Löhneysen, Phys. Rev. B **76**, 045117 (2007).
[20] H. Aoki, S. Uji, A. K. Albessard, and Y. Ōnuki, Phys. Rev. Lett. **71**, 2110 (1993).
[21] R. A. Neifeld, M. Croft, T. Mihalisin, C. U. Segre, M. Madigan, M. S. Torikachvili, M. B. Maple, and L. E. DeLong, Phys. Rev. B **32**, 6928 (1985).
[22] M. Yano, A. Sekiyama, H. Fujiwara, Y. Amano, S. Imada, T. Muro M. Yabashi, K. Tamasaku, A. Higashiya, T. Ishikawa, Y. Ōnuki, and S. Suga, Phys. Rev. B **77**, 035118 (2008).

[23] S. Quezel, J. Rossat-Mignot, B. Chevalier, P. Lejay, and J. Etorneau, Solid State Commun. **49**, 685 (1984).
[24] B. H. Grier, J. M. Lawrence, V. Murgai, and R. D. Parks, Phys. Rev. B **29**, 2664 (1984).
[25] T. Graf, M. F. Hundley, R. Modler, R. Movshovich, J. D. Thompson, D. Mandrus, R. A. Fisher, and N. E. Phillips, Phys. Rev. B **57**, 7442 (1998).
[26] S. Kawarazaki, M. Sato, Y. Miyako, N. Chigusa, K. Watanabe, N. Metoki, Y. Koike, and M. Nishi, Phys. Rev. B **61**, 4167 (2000).
[27] J. Thompson, R. Parks, and H. Borges, J. Magn. Magn. Mater. **54–57**, 377 (1986).
[28] R. Movshovich, T. Graf, D. Mandrus, J. D. Thompson, J. L. Smith, and Z. Fisk, Phys. Rev. B **53**, 8241 (1996).
[29] S. Araki, M. Nakashima, R. Settai, T. C. Kobayashi, and Y. Onuki, J. Phys. Condens. Matter **14**, L377 (2002).
[30] N. D. Mathur, F. M. Grosche, S. R. Julian, I. R. Walker, D. M. Freye, R. K. W. Haselwimmer, and G. G. Lonzarich, Nature (London) **394**, 39 (1998).
[31] F. Grosche, S. Julian, N. Mathur, F. Carter, and G. Lonzarich, Physica B **237**, 197 (1997).
[32] M. Berisso, P. Pedrazzini, J. Sereni, O. Trovarelli, C. Geibel, and F. Steglich, Europ. Phys. B **30**, 343 (2002).
[33] R. Settai, A. Misawa, S. Araki, M. Kosaki, K. Sugiyama, T. Takeuchi, K. Kindo, Y. Haga, E. Yamamoto, and Y. Ōnuki, J. Phys. Soc. Jpn. **66**, 2260 (1997).
[34] S. Araki, R. Settai, T. C. Kobayashi, H. Harima, and Y. Ōnuki, Phys. Rev. B **64**, 224417 (2001).
[35] M. Besnus, J. Kappler, P. Lehmann, and A. Meyer, Solid State Commun. **55**, 779 (1985).
[36] P. Haen, F. Lapierre, J. Kappler, P. Lejay, J. Flouquet, and A. Meyer, J. Magn. Magn. Mater. **76–77**, 143 (1988).
[37] J. Boucherle, F. Givord, S. Raymond, J. Schweizer, E. Lelievre-Berna, P. Lejay, and G. Fillion, J. Phys. Condens. Matter **13**, 10901 (2001).
[38] The sign of B_4^4 determines the signs of α and/or β, i.e., the rotation of the orbital. However, neither macroscopic nor neutron scattering or XAS are sensitive to the signs of α and/or β.
[39] H. Abe, H. Kitazawa, H. Suzuki, G. Kido, and T. Matsumoto, J. Magn. Magn. Mater. **177–181**, 479 (1998).
[40] V. Vildosola, A. M. Llois, and M. Alouani, Phys. Rev. B **71**, 184420 (2005).
[41] P. Hansmann *et al.*, Phys. Rev. Lett. **100**, 066405 (2008).
[42] T. Willers *et al.*, Phys. Rev. B **80**, 115106 (2009).
[43] T. Willers *et al.*, Phys. Rev. B **81**, 195114 (2010).
[44] J. C. Fuggle, F. U. Hillebrecht, Z. Zołnierek, R. Lässer, C. Freiburg, O. Gunnarsson, and K. Schönhammer, Phys. Rev. B **27**, 7330 (1983).
[45] O. Gunnarsson and K. Schönhammer, Phys. Rev. B **28**, 4315 (1983).
[46] A. Tanaka and T. Jo, J. Phys. Soc. Jpn. **63**, 2788 (1994).
[47] A. Murani, J. Phys. C **16**, 6359 (1983).
[48] With the present resolution the data are equally well described with an inelastic or quasielastic Lorentzian line.
[49] E. A. Goremychkin and R. Osborn, Phys. Rev. B **47**, 14280 (1993).
[50] N. H. van Dijk, B. Fåk, T. Charvolin, P. Lejay, and J. M. Mignot, Phys. Rev. B **61**, 8922 (2000).
[51] Y. Kawasaki, K. Ishida, Y. Kitaoka, and K. Asayama, Phys. Rev. B **58**, 8634 (1998).
[52] N. E. Bickers, D. L. Cox, and J. W. Wilkins, Phys. Rev. B **36**, 2036 (1987).
[53] F. Steglich, P. Hellmann, S. Thomas, P. Gegenwart, A. Link, R. Helfrich, G. Sparn, M. Lang, C. Geibel, and W. Assmus, Physica B **237**, 192 (1997).
[54] P. Link and D. Jaccard, Physica B **230**, 31 (1997).
[55] M. Matsumoto, M. J. Han, J. Otsuki, and S. Y. Savrasov, Phys. Rev. Lett. **103**, 096403 (2009).